Structure, Vol. 13, 617-627, April, 2005, © Elsevier Ltd All rights reserved. DOI 10.1016/j.str.2005.01.021

# Mechanism of a molecular valve in the halorhodopsin chloride pump.

**Andreea D. Gruia[1], Ana-Nicoleta Bondar[1,2], Jeremy C. Smith[2] and Stefan Fischer[1*]**

[1] Computational Biochemistry
[2] Computational Molecular Biophysics

IWR, Heidelberg University,
Im Neuenheimer Feld 368,
D-69210 Heidelberg, Germany

## Summary

**Halorhodopsin is a light-driven chloride anion pump in which the *trans→cis* photoisomerization of a retinal chromophore triggers a photocyle resulting in the translocation of chloride across the plasma membrane. The mechanism of chloride transfer past the *cis* retinal is determined here by computing multiple pathways for this process. The calculations reveal two conditions of the valve mechanism. First, a lumen absent in the ground state structure is transiently opened by chloride passage. Second, this activated opening, which is achieved by flexible deformation of the surrounding protein, is shown to significantly raise the chloride translocation barrier between photocycles, thus preventing chloride backflow. Unlike macroscopic valve designs, the protein allows differential ion flows in the pumping and resting states that are tuned to match the physiological timescales of the cell, thus creating a 'kinetic' valve.**

## Introduction

Ion pumps are fundamental for converting and storing energy in living systems. Using an external energy source, the pumps translocate ions across the membrane, thus building electrochemical gradients, which then serve to drive physiological processes such as ATP synthesis or propagation of action potentials along axons. Ion pumps are sophisticated molecular machines, which must accomplish several functions: in addition to driving the ionic transport, they must possess valve mechanisms that prevent dissipation of the ion gradients they create. How such molecular valves are designed at the molecular level is hitherto unclear. Here we examine this question by performing molecular mechanics simulations of halorhodopsin, the only anionic pump for which an atomic-resolution three-dimensional structure exists so far.

Halorhodopsin is a member of the family of light-activated retinal proteins found in the membrane of Haloarchaea. The role of this light-driven inward-directed chloride pump is to maintain osmotic pressure during cell growth (Schobert et al., 1982, Oesterhelt, 1995). Halorhodopsin shares high sequence homology with bacteriorhodopsin, a light-driven proton pump which possesses the same topology (Mukohata et al., 1999, Ihara et al., 1999): seven transmembrane helices (see Fig. 1A) and one retinal chromophore covalently attached via a protonated Schiff base linkage to a lysine on helix G (Oesterhelt, 1995, Alshuth et al., 1985). Absorption of green light by the retinal in the all-trans configuration (Fig. 1B) is followed by isomerization of the C13=C14 double bond to cis. After relaxation to the electronic ground state the protein is left in a high-energy configuration, initiating a photocycle during which gradual release of the energy is used to transfer chloride ions between different binding sites, resulting in the net translocation of one chloride from the extracellular to the cytoplasmic side of the membrane (Váró et al., 1995a, Losi et al., 2001).

Several kinetic models of the photocycle involving branching pathways or different numbers of early intermediates have been suggested (Lanyi, 1990). A simplified scheme that agrees with most of the available spectroscopic and kinetic data has been proposed for halorhodopsin of *Halobacterium salinarum* (Váró et al., 1995b, Oesterhelt et al., 1985):

$$HR_{578} \xrightarrow{\sim 5\ ps} HR_{600} \xrightarrow[(1)]{1\ \mu s} HR_{520} \xrightarrow[(2)]{\sim 4\ ms} HR_{640} \xrightarrow[(3)]{\sim 10\ ms} HR_{578}$$

where the subscripts indicate absorption wavelengths and steps 1 to 3 correspond to the chloride transfer steps shown in Fig. 1A. Formation of each spectroscopic intermediate in the photocycle is coupled to charge motions in the protein (mostly chloride translocation), as shown by photovoltaic experiments (Kalaidzidis et al., 1998, Ludmann et al., 2000). Such experiments however do not provide the exact location of the chloride at each step of the photocycle. The only unambiguous chloride position is known for the ground state HR578, which has been crystallized (Kolbe et al., 2000). In this crystal structure, the chloride is proximal to the all-trans retinal whose protonated Schiff base points towards the extracellular side (Fig. 1C). There, the deeply-buried anion is stabilized by electrostatic interactions with the positively-charged Schiff base and Arg108, as well as by three water molecules and by the hydroxyl groups

* Correspondence: Stefan.Fischer@iwr.uni-heidelberg.de

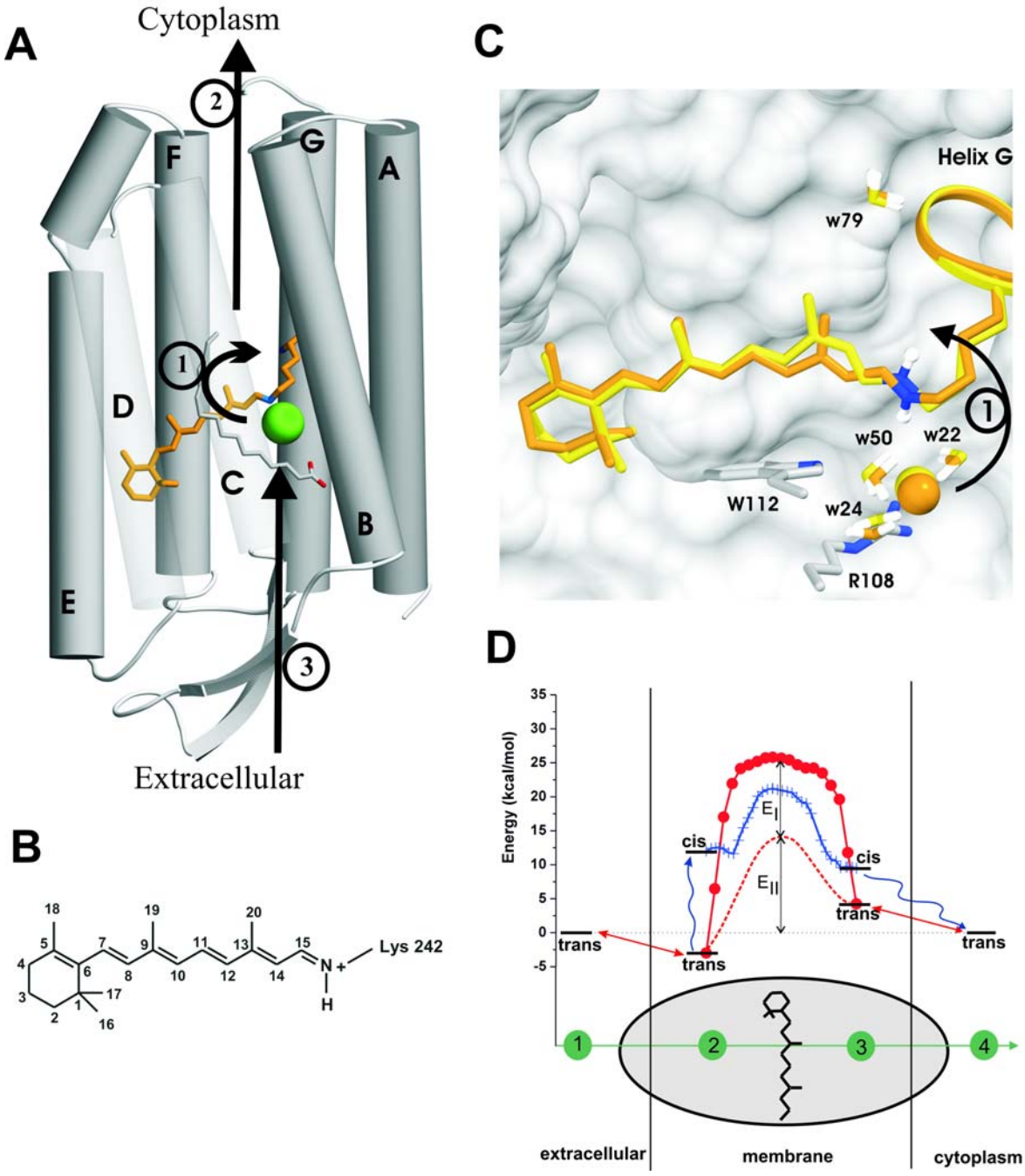


**Figure 1**. The primary chloride transfer step.
**A)** Arrows indicate the direction of chloride transfer through halorhodopsin: photocycle steps 1, 2 and 3 (see Introduction) correspond respectively to passage past retinal, chloride release and chloride uptake. The ground state structure is shown, with the chloride (green sphere) below the Schiff base nitrogen (blue) of the all-*trans* retinal (orange). A palmitate molecule (grey) is seen in the crystal. **B)** Retinal in all-*trans* configuration showing the Schiff base linkage to Lys242. **C)** The crystallographic all-*trans* ground state is shown in orange. The reactant state of the primary chloride transfer (step 1) with retinal in 13-*cis* is in yellow. The chloride ion is shown as sphere and the inner surface of the protein is in grey (nearby waters are numbered as in the crystal, PDB entry 1E12). **D)** Kinetic valve mechanism. Chloride positions 1 and 4 represent solvated chloride on either side of the membrane. Positions 2 and 3 represent chloride bound to either side of retinal (as in Fig. 2B and 2C, respectively). The energy levels of three chloride translocation scenarios are shown: I) During active pumping (wavy blue curve), the all-*trans* to 13-*cis* retinal photoisomerization stores about 15 kcal/mol in the protein (Losi et al., 2001), while chloride is in position 2. This is followed by the primary chloride transfer (+ + +, from path **2**) over a small 9 kcal/mol barrier (i.e., open valve) to position 3 and gradual relaxation as chloride moves into the cytoplasm (position 4). II) Between pumping cycles (full red curve), chloride reversibly binds to position 2 near all-*trans* retinal (binding–energy is -3kcal/mol, Schobert et al., 1984). This is followed by chloride passage past retinal (●●●, values from the computed MEP) over a large 28 kcal/mol barrier and unbinding on the cytoplasmic side of the membrane. The barrier for backflow is 28-3=25 kcal/mol, i.e., the valve is kinetically closed. III) Chloride leakage (dotted red line) in the hypothetical absence of the energetic cost of lumen opening ($E_I$=10 kcal/mol), which would result in a backflow barrier $E_{II}$ of only 15 kcal/mol.

of several serine side chains (Kolbe et al., 2000, Braiman et al., 1994). An essential step of the photocycle after retinal isomerization is the translocation of chloride away from this binding site, with the chloride passing from below to above the retinal as viewed in Fig. 1C. This primary transfer step, which constitutes the focus of the present paper, has been proposed to be driven by electrostatic interactions between the chloride anion and the positively-charged Schiff-base, whose N-H bond has been reoriented towards the cytoplasmic side by the photoisomerization (Lanyi, 1984, Dér et al., 1985, Ames et al., 1992, Warshel, 1978). Based on FTIR and photoelectric measurements, the microsecond decay of the $HR_{600}$ intermediate to $HR_{520}$ (step 1) has been assigned to the primary chloride transfer step (Kalaidzidis et al., 1998, Ludmann et al., 2000, Kolbe et al., 2000, Walter et al., 1994).

The crystal structure of ground-state halorhodopsin raises several important questions regarding the mechanism of primary chloride transfer. Firstly, there is no space around retinal wide enough for a chloride ion to pass (see Fig. 2A). How, then, does the protein open a passage, and on which side of retinal (on the side of Ser115 or of Asp238, see Fig. 2B) ? Secondly, what are the rate-limiting factors that are responsible for the microsecond timescale of this process, for example, which residues play a role in raising/lowering the corresponding activation barrier ? Finally, an important feature of halorhodopsin as a pump is to be able to prevent chloride backflow in the resting state. For this purpose, the protein must possess one or several molecular valves that hinder the chloride leakage between pumping cycles and open when the protein is light-activated. Is such a valve involved in the primary chloride transfer step ?

To address these questions, we have used an efficient method (Fischer and Karplus, 1992) for computing Minimum Energy Paths (MEP) in proteins to exhaustively search for chloride transfer pathways. These MEPs describe the motion of the chloride ion and of the surrounding protein, for which all degrees of freedom are energy optimized. When entropy changes are negligible, which has been shown to be the case for the primary chloride transfer (Váró et al., 1995a, Losi et al., 2001), the MEPs with the lowest-energy barriers are the most probable pathways. These trajectories can be followed as molecular movies (available under http://www.iwr.uni-heidelberg.de/groups/biocomp/fischer). The calculations reveal that: 1) Chloride pathways on the Ser115 side of retinal have activation barriers consistent with experiment, while pathways on the Asp238 side are energetically forbidden. Pathways computed for the Ser115Ala mutant are found to have barriers similar to the wild-type, explaining the phenotype of this mutation. 2) Long-range protein flexibility allows the transient opening of a passage for chloride through collective displacement of nearby helices, which is facilitated by built-in 'breaking-points'. 3) Pathways computed in the ground state of the protein show that this activated opening constitutes a conceptually-new kinetic valve mechanism by which backflow of chloride anions is slowed down between pumping cycles.

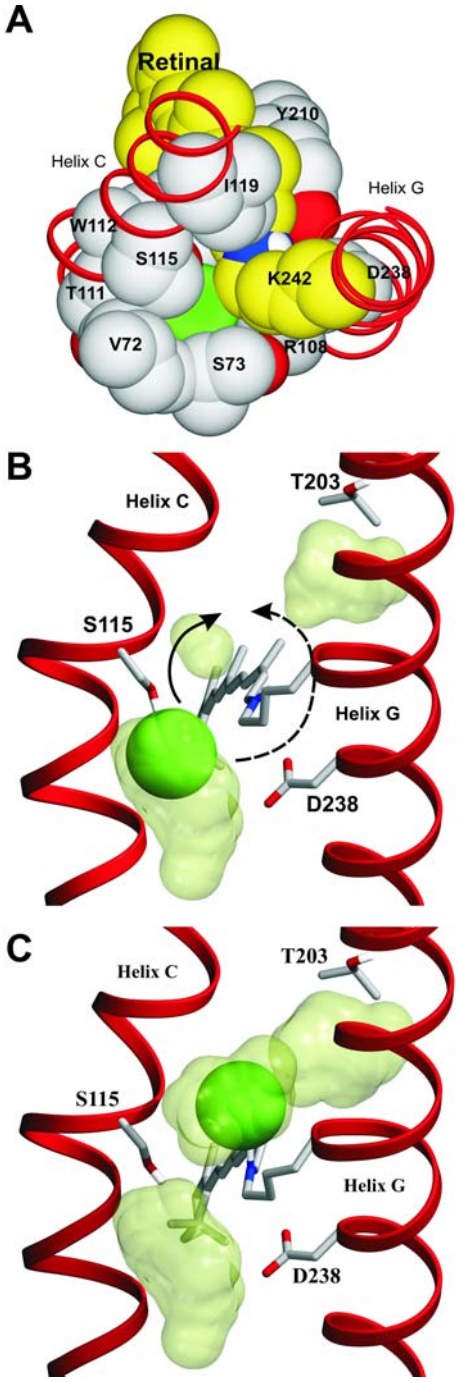


**Figure 2**. Chloride passage past 13-*cis* retinal.
**A)** The reactant state of primary chloride transfer, viewed from the cytoplasmic side, showing that the passage from the extracellular side is too narrow for chloride (Van der Waals radius of 2.27 Å, in green). Retinal and Lys242 are in yellow (Schiff base nitrogen in blue). Oxygens of surrounding sidechains are in red. **B)** Cavities (light green) for chloride (dark green) and waters (not shown) in the reactant state. Arrows indicate putative routes for chloride on the Ser115 or on the Asp238 side of the retinal. **C)** Cavities in the product state, showing the chloride in its most stable position above retinal (see Methods).

## Results

***Transfer end-states.*** In the absence of published crystal structures corresponding to the end states of the primary chloride transfer, which both have retinal in 13-cis, these were derived from the all-trans ground state crystal structure. This is feasible because no major conformational change is expected to occur between these states, given the fast timescale of the early steps of the photocycle and that illumination of the ground state crystal initiates a photocycle without breaking the crystal (D.Oesterhelt, personal communication). The reactant state was built by replacing in one monomer the coordinates of retinal and Lys242 with those of 13-cis retinal from the crystal structure of the K intermediate of bacteriorhodopsin (PDB code 1 QKO) (Edman et al., 1999). The structure was then subjected to energy minimization to allow relaxation of the protein environment around the 13-cis retinal. The resulting structure is very similar to the ground state (Fig. 1C), with a root mean square deviation of only ~0.3 Å. The chloride position remains unchanged, consistent with FTIR data showing maintenance of the anion-Arg108 interaction in the $HR_{600}$ intermediate (Braiman et al., 1994). The structure is also very similar to the crystal structure of an $HR_{600}$ state (Gmelin, 2003).

The product state structure was derived from the reactant state by moving the chloride into different sites above the 13-*cis* retinal. Two sites could accommodate the anion. One position near Thr203 has been suggested based on the observation that the Thr203Val mutation abolishes chloride transport (Rüdiger et al., 1997). A cavity large enough to accommodate the chloride ion is indeed present below Thr203 (see Fig. 2B). However, this 'Thr203 site' would not be consistent with FTIR and Raman spectroscopic data (Walter et al., 1994, Gersher et al., 1997), according to which, early in the photocycle, the chloride moves closer to the Schiff base with which it establishes a stronger interaction in $HR_{520}$ than in $HR_{600}$. A location consistent with the FTIR/Raman data is inside a small cavity between retinal and Ser115 (Fig. 2C). There, the chloride makes a salt bridge with the Schiff base. The potential energy of the 'Thr203' site is 17 kcal/mol higher than that of the 'Ser115 site'. To account for a difference in the solvation self-energy of the chloride the Poisson-Boltzmann equation was solved (see Methods) with chloride in each of the two sites. The solvation self-energy was found to be 4 kcal/mol in favor of the chloride position near Thr203, which is located slightly closer to the bulk solvent than Ser115. The sum of potential and solvation energy is thus 13 kcal/mol in favor of the chloride being in the 'Ser115 site', which was used for the present product state.

The differences between the initial (reactant) and final (product) states of the primary transfer step are small. The three water molecules that hydrate the chloride ion in the reactant (Fig. 1C) reorient in the product so as to establish more favorable hydrogen bonds with each other and neighboring residues. In the product state the Schiff base twists towards the chloride (compare Panels B and C in Fig. 2) and water w79 moves towards the retinal and establishes a hydrogen bond with the chloride ion (not shown). The calculated energy difference between the product and reactant structures is small at -2.5 kcal/mol, close to experimental values of -0.5 and -2.5

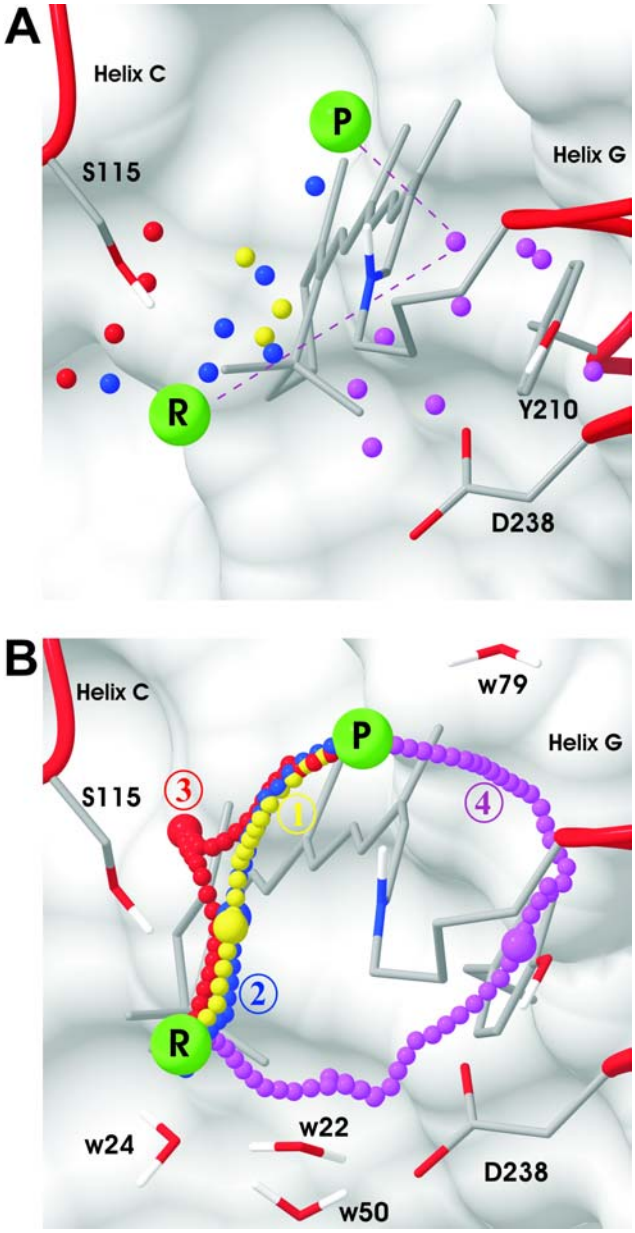


**Figure 3**. Searching for Minimum Energy Pathways (MEPs). **A)** The 23 randomly-placed intermediate chloride positions (small spheres) used to build different initial guesses of the path by linear interpolation (dotted line, shown only for one path) from the reactant (R) to the product (P) chloride position (large green spheres). Color coding of the small spheres indicates into which of the four different MEPs (see Panel B) each initial path will be refined. **B)** Positions of chloride along the four different MEPs (chain of small spheres, the bigger sphere indicating the transition state) that result from Conjugate Peak Refinement of the 23 initial paths described in Panel A: path **1** (yellow), path **2** (blue), path **3** (red) and path **4** (purple). In both panels the protein is in the product conformation, its inner surface shown in grey.

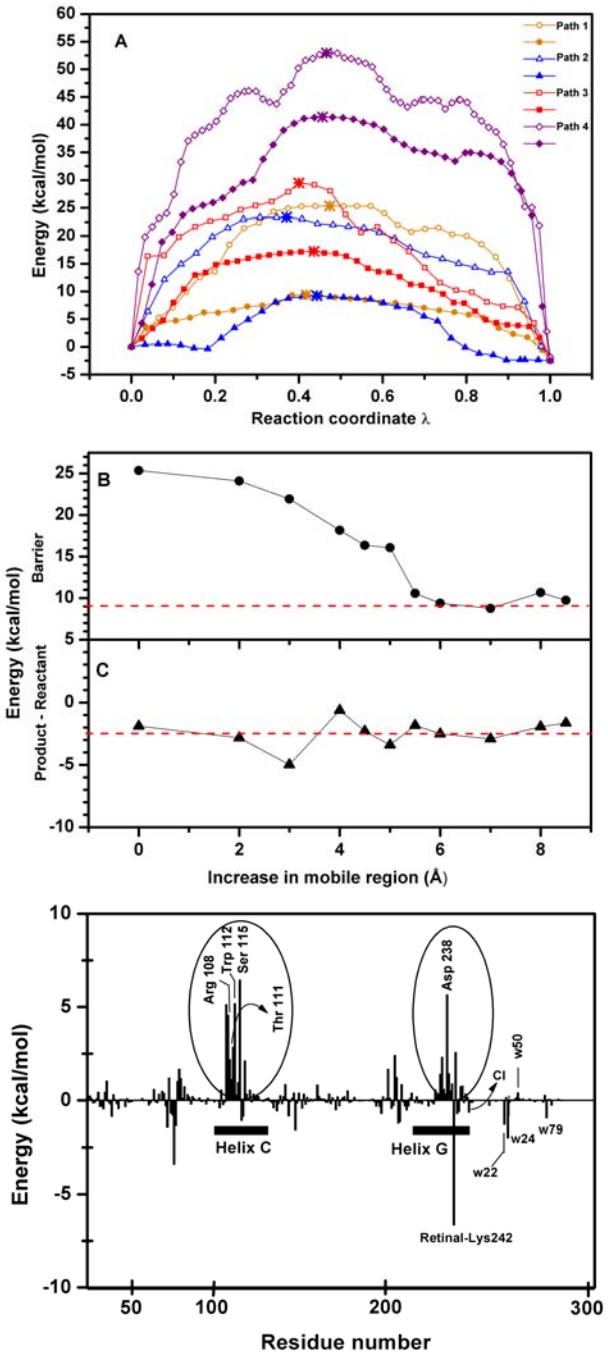


**Figure 4**. Role of protein flexibility.
**A)** Energy profile along the four MEPs (see Fig. 3B) computed either with a 'core region' (open symbols) or with an 'extended region' (filled symbols) of mobile atoms around the retinal (the regions are defined in Methods). The transition-states are indicated by a *. The reaction coordinate λ is the normalized sum up to any given point along the path of the change in all atomic coordinates, measured as an RMS difference (Fischer and Karplus, 1992). **B)** and **C)** Barrier height and energy difference between optimized reactant and product structures of path **1** as a function of the size of the mobile region (additional distance around the 'core region', see text). The experimental enthalpies are indicated by dashed lines. **D)** Contribution from individual protein residues to the energy barrier of path **2**. For a given residue, this is the sum of the self-energy of that residue plus half the interaction-energy between that residue and the rest of the system.

kcal/mol obtained for the energy difference between $HR_{520}$ and $HR_{600}$ in salinarum and pharaonis halorhodopsins, respectively (Váró et al., 1995a, Losi et al., 2001, Váró et al., 1995b). Decomposition of the energy function reveals that the favorable interactions of the chloride with its hydrating water cluster, Arg108 and Ser115 in the reactant state are compensated in the product by the increased distance between the chloride and the negatively-charged Asp238, as well as by the improved interactions of the anion with the Schiff base and water w79. In this way, the protein achieves one important objective of the first transfer step, which is to prevent too much dissipation of the energy stored after photoisomerization, thus keeping the protein 'activated' enough to drive the subsequent transfer steps (2 and 3, see Fig. 1A) of the photocycle. Interestingly, once in the product conformation, a passage for chloride to the cavity near Thr203 is partially opened (Fig. 2C), possibly preparing the next step of chloride transfer. However, whether the 'Thr203 site' would correspond to a long-lived intermediate is unclear.

***Searching for pathways***. Like in the crystal structure of the all-*trans* ground state, the reactant and product structures are tightly packed around the 13-*cis* retinal, allowing no passage for chloride translocation past the chromophore (Fig. 2A). Two types of route for chloride passage are conceivable (see Fig. 2B): one passes between helix C and the retinal (the 'Ser115 side'), the other between helix G and the retinal (the 'Asp238 side'). For either route, the chloride could pass by various places along the retinal chain. Twenty-three different chloride routes were each approximated by an initial path in which the chloride route goes through a randomly-chosen position around retinal, as shown in Fig. 3A. Each initial path was refined into the nearest MEP by the Conjugate Peak Refinement (CPR) algorithm (see Methods) (Fischer and Karplus, 1992). The resulting twenty-three MEPs clustered into only four distinct pathways (labeled **1** to **4**), each of which is characterized by a different saddle-point of the energy-surface, *i.e.*, by a different transition-state structure. The trajectories followed by the chloride along these four paths are shown in Fig. 3B. Paths **1** to **3** have chloride routes on the Ser115 side, whereas path **4** has the chloride passing on the Asp238 side.

***Role of protein flexibility.*** The energy barriers along the four pathways, whose energy profiles are shown in Fig. 4A, depend on the amount of protein flexibility allowed during the path calculations. When a region of 46 residues around retinal (called here the 'core region', see Methods) is allowed to be mobile, but the remaining atoms are fixed, the energy barriers of all four pathways exceed 23 kcal/mol (Table 1). This is much too high for a process that occurs on the microsecond timescale. To test whether more protein flexibility would facilitate the opening of a passage for

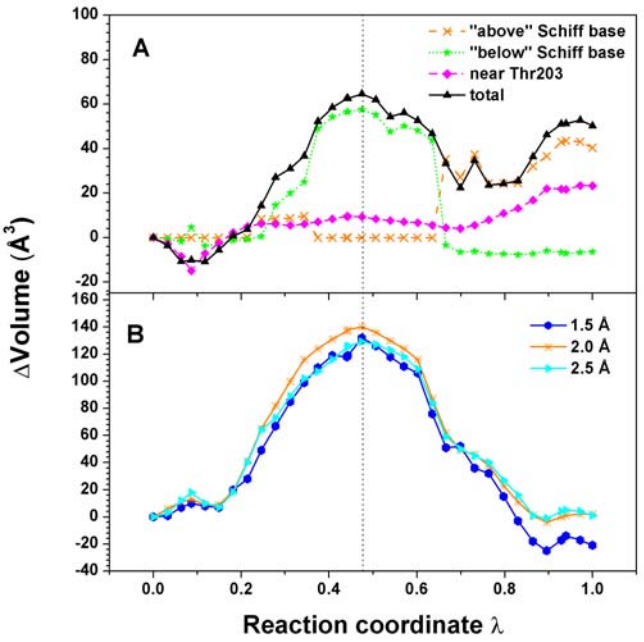


**Figure 5** . Protein "breathing" allows transient lumen opening.
**A)** Changes in the volume of cavities nearby the retinal during the chloride transfer of path **2**. The cavity "below" the Schiff base holds the chloride in the reactant state (see Fig. 2B), the cavity directly "above" the Schiff base holds the chloride after transfer (Fig. 2C). The cavity near Thr203 is visible in Fig. 2B and C. The "total" volume of these 3 cavities is plotted. The cavity boundaries were taken as the contact point of a rolling sphere (radius 1.3 Å) in absence of the chloride and water molecules inside them. **B)** Corresponding change in the overall volume of the protein (i.e., halorhodopsin monomer and its cavities). The protein boundary was taken as the contact point of a rolling sphere (different radii, see inset), in presence of the chloride and water molecules. The reaction coordinate λ is described in Fig. 4A, its value at the transition state is shown by a vertical dashed line.

chloride by lowering the barrier, the mobile region was extended: path **1** was recomputed with atoms up to an additional 8.5 Å radius around the 'core region' allowed to be mobile (thus encompassing almost the entire halorhodopsin monomer). Fig. 4B shows that the energy barrier decreases and stabilizes around a value of 9 kcal/mol as the size of the mobile region increases. This barrier is consistent with a microsecond timescale (assuming Eyring's standard rate law $k_BT/h \exp[-\Delta E^{\ddagger}/k_BT]$, where $k_B$, h and T are the Boltzmann constant, the Planck constant and the temperature, respectively) and is close to the experimental enthalpy of activation of 8±2 kcal/mol measured for the homologous *pharaonis* halorhodopsin (Váró et al., 1995a, Losi et al., 2001). It is noteworthy that this decrease in barrier height is not simply due to a decrease in the energy of the product relative to the reactant, which could pull down the barrier artificially. Indeed, the energy difference between the geometry-optimized reactant and product states remains near the experimental value for any extent of the mobile region, as shown in Fig. 4C.

Since the barrier height converges for mobile regions of 5.5 Å or more around the 'core region' (*i.e.*, about 10 Å around the Schiff base), an 'extended region' of mobile atoms consisting of the 'core region' plus a layer of 6 Å was used to re-compute MEPs for all twenty-three initial guess paths. The resulting MEPs cluster again into only four distinct pathways whose chloride routes are essentially the same as obtained with the mobile 'core region'. However, the increase of the mobile region leads to a significant decrease of the energy barrier for all four pathways, as seen in Table 1. These pathways are described in the next sections and are available as molecular movies (see the web-address above).

Table 1. Energy barriers for the primary chloride transfer (kcal/mol).

| | $\Delta E^{\ddagger}$ ('core region')[a] | $\Delta E^{\ddagger}$ ('extended region')[a] |
|---|---|---|
| Path 1 | 25.3 | 9.4 |
| Path 2 | 23.3 | 9.2 |
| Path 3 | 29.4 | 17.2 |
| Path 4 | 52.9 | 41.3 |

[a]Region around retinal allowed to move (see text)

***Ser115-routes.*** In paths **1**, **2** and **3** the chloride moves past the retinal on the side of Ser115 (see Fig. 3B). Paths **1** and **2** have the lowest energy barriers (Table 1), which are consistent with experiment (Váró et al., 1995a, Losi et al., 2001). Both pathways have similar chloride routes and the same sequence of events, which is as follows. First, the chloride moves up towards the Schiff base. For this, the lumen between retinal, Ser115 and Ser73 (seen in Fig. 2A) enlarges transiently. Meanwhile, the chloride maintains its hydrogen bonds with water molecule w24 and the hydroxyl group of Ser115, which both accompany the anion until after the transition state is passed and the lumen starts reclosing. These hydrogen bonds are replaced by a salt bridge with the Schiff base, which twists towards the chloride while water w24 returns to its starting position, and by a hydrogen bond with water w79, which moves towards the retinal while the hydroxyl group of Ser115 returns to its reactant orientation.

The total volume of the three cavities near the retinal Schiff base (shown in Fig. 2B and C) transiently increases by up to 65 $Å^3$, so as to allow the opening of the lumen. This is only slightly more than the volume of a chloride van der Waals sphere (~50 $Å^3$). Figure 5A shows that the maximum volume increase is reached when the chloride is in the transition state position, i.e., when the energy is maximal. The lumen forms by transiently extending a shaft from the cavity "below" the Schiff base (see Fig. 2B), following which the cavity returns to its original volume. The small cavity directly "above" the Schiff base has to increase by about 40 $Å^3$ to accommodate the chloride in the product configuration. In the product state the cavity situated near Thr203 also increases by about 25 $Å^3$ relative to the pre-transfer state.

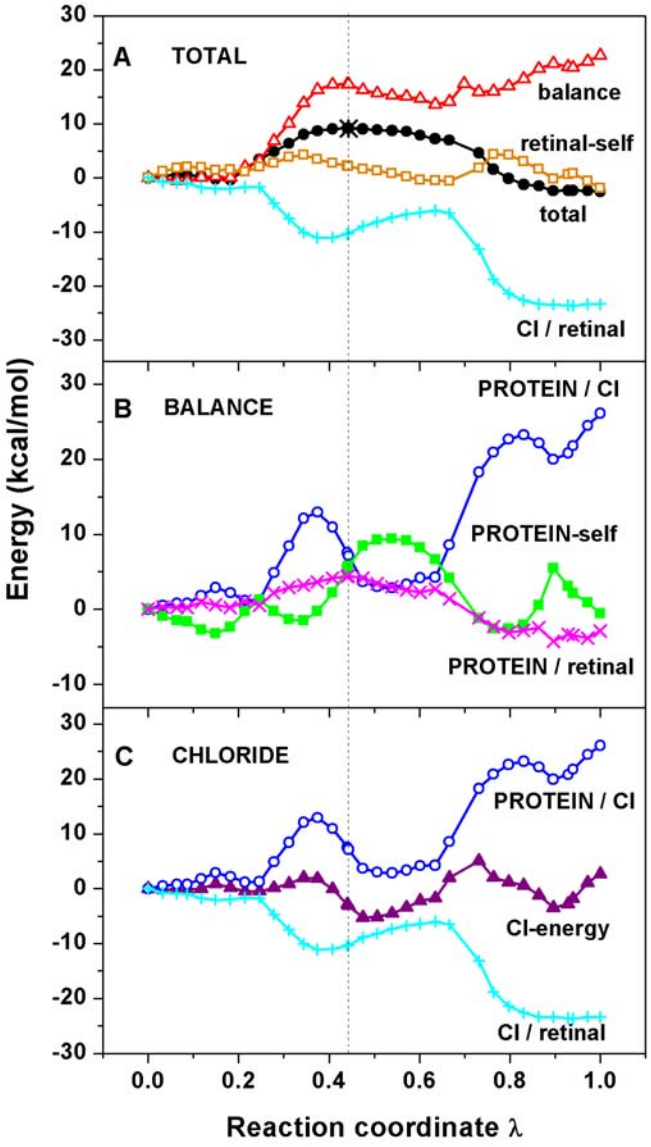


**Figure 6** . Energy decomposition.
**A)** The total energy along path **2** (●) is decomposed into the retinal self-energy (□), the chloride/retinal interaction energy (+) and the remainder of the energy terms ('balance', Δ). **B)** The 'balance' term of Panel A is decomposed into interactions of the PROTEIN (everything except chloride and retinal) with chloride (○), with retinal (x) and with itself (green ■). **C)** The chloride-energy (▲) is the sum of two interaction terms: Cl/retinal (+, same as in Panel A) and PROTEIN/Cl (○, same as in Panel B). The reaction coordinate λ is described in Fig. 4A, its value at the transition state is shown by a vertical dashed line.

In path **3** the chloride route first goes towards the ionone ring of retinal and then passes behind the sidechain of Ser115 (as viewed in Fig. 3B). Thus, the distance between the chloride anion and the Schiff base increases until the transition state is reached, unlike in paths **1** and **2** in which this distance is shorter at the transition state than in the reactant. Consequently, the electrostatically-favorable chloride/Schiff base interaction does not contribute to lowering the energy barrier in path **3**, whereas it does so in paths **1** and **2**. At the transition state of path **3** the Schiff base twists significantly towards Asp238 so as to establish a salt-bridge. This is not enough, though, to compensate the weaker chloride/Schiff base interaction and results in a high energy barrier of 17.2 kcal/mol, which indicates that path 3 is unlikely.

***Energy decomposition.*** To better understand the relative roles played by the chloride (Cl), the retinal (including the sidechain of Lys242), and the rest of the protein (including water and palmitate molecules, denoted here as PROTEIN), the potential energy along the preferred pathway (path 2) was decomposed into 5 terms: two self-energies (retinal-self and PROTEIN-self, the self-energy of chloride being zero here) and three interaction energies (Cl/retinal, PROTEIN/Cl and PROTEIN/retinal). In Fig. 6A the Cl/retinal interaction term is seen to gradually decrease by 25 kcal/mol along the path, reflecting the increasingly favorable interaction of the anion with the positively-charged Schiff base as this ion-pair distance decreases. This confirms that the increased ion-pair separation resulting from retinal photoisomerization is the 'driving force' for the primary chloride transfer, as proposed in previous theoretical studies (Warshel, 1978). It is also the only term that contributes to lowering the energy barrier at the transition state (located at λ=0.44 Å in Fig. 6). In contrast, the retinal-self term undergoes minor variations along the path, indicative of negligible strain in the retinal chain during the transfer. The three remaining terms constitute the 'balance' in Fig. 6A. Each of these contributes to raising the barrier (Fig. 6B), although their local maxima occur shortly before, at or shortly after the transition state (at λ=0.36, λ=0.44 and λ=0.53, respectively for PROTEIN/Cl, PROTEIN/, retinal and PROTEIN-self), this out-of-phase behavior lowering their summed contribution to the barrier. The positive value of these terms at the transition state is due mostly to the strain induced in the protein by the enlarging of the lumen, adding at least 10 kcal/mol to the barrier. Indeed, the potential energy of the chloride anion (composed of the Cl/retinal and the PROTEIN/Cl terms) has only small fluctuations along the path (Fig. 6C), thus showing that the chloride motion is relatively unhindered once the opening of the lumen has been achieved. This means that the process governing the rate of chloride transfer is the thermally-activated fluctuation of the protein matrix that transiently opens the cavity of the lumen, the chloride then diffusing rather quickly past the retinal. It has been recently proposed that a similar role is played by cavity formation in bacteriorhodopsin, where the transient opening and hydration of a hydrophobic shaft might be the rate-limiting step for proton transfer along that shaft (Friedman et al, 2003).

***Molecular valve mechanism.*** The fact that the lumen opening adds more than 10 kcal/mol to the barrier of the chloride transfer, which otherwise would be nearly

barrier-less, raises the question of why the architecture of halorhodopsin did not evolve a less constricted passage for chloride. As for any pump, halorhodopsin must have some valve mechanism to prevent backflow in the resting state, i.e., chloride flow should be impeded while a given halorhodopsin molecule waits to be activated by the next photon. Two types of valves are conceivable, depending on how they close: 'check' valves, which impede flow in only one direction, and 'throttle' valves, which impede flow equally in both directions. To test whether the activated lumen opening plays the role of a spring in a throttle valve, the pathway for chloride passage past all-trans retinal (i.e., the resting state between pumping cycles) was computed. The resulting chloride route with the lowest barrier is very similar to that described above for path 2 and exhibits a similar dependence of the barrier height on the amount of allowed protein flexibility (as seen in Fig. 4B). It involves the opening of a lumen by the passage of the anion (not shown here, available as movie). However, its energy barrier is 28 kcal/mol (red curve with ●●● in Fig. 1D), which corresponds to a timescale of hours. This indicates that, in the resting state, chloride transfer towards the cytoplasm is kinetically prohibited. Energy decomposition reveals that flexible lumen opening contributes about 10 kcal/mol to this barrier height. Thus, if the lumen were to be permanently open or its opening were to require no energy, the barrier height of the chloride transfer in the all-trans resting state would be only 28-10=18 kcal/mol. Taken relative to the state of chloride in solution, whose energy (from the experimentally-determined dissociation constant of 10 mM, Schobert et al., 1984) is 3 kcal/mol higher than that of the bound chloride, the transfer barrier in absence of the lumen opening energy would be only 18-3=15 kcal/mol (red dashed curve in Fig. 1D). This corresponds to a timescale of milliseconds, which would represent a high rate of chloride leakage. Thus, the forced opening of the lumen slows down chloride backflow in the resting state. This suggests that the constricted passage past retinal plays the role of a kinetic valve: In the all-trans state, chloride passage takes hours, so that from a physiological point of view the valve can be considered 'closed' between pumping photocycles. After the protein has been light-activated, the 9 kcal/mol energy barrier due to lumen opening in the high-energy 13-cis state (blue curve in Fig. 1D) still slows down primary chloride transfer, but the microsecond timescale is fast enough relative to other steps of the photocycle so that the valve can be considered as 'open' during pumping. The flexible constriction thus plays the role of the spring in this molecular throttle valve.

***Structural basis of the spring.*** The molecular movies of paths **1** and **2** show that chloride opens the lumen by moving between Trp112 (on helix C, Fig 1C) and Lys242 (on helix G), thereby pushing aside helix C (and to a lesser extent helix G). Indeed, decomposing the energy barrier into contributions from individual residues (Fig. 4D) reveals that two clusters of residues belonging to helices C and G are energetically responsible for most of the energy barrier. Further decomposition shows that these residues contribute mainly by an increase in their self-energy (*i.e.*, the sum of interactions within the residue) and less favorable interactions with the protein, rather than by less favorable interactions with the chloride. This reflects significant strain of helices C and G, whose collective motion is necessary for the passage opening. This motion is facilitated on helix C by a kink (see Fig. 2B) present near Pro117 that confers a $3_{10}$ helix conformation on residues 110-113, a structural feature that distinguishes halorhodopsin from other retinal proteins (Essen, 2002). This kink is located at the level where the helix flexes most upon passage of the chloride, suggesting a role for this conserved proline as a pre-determined 'breaking point' that gives helix C the flexibility required for the primary transfer step. A similar bend in helix C was seen in a crystal structure of the L intermediate of bacteriorhodopsin (Edman et al., 2004), in which the local flexibility necessary for the primary proton transfer is facilitated by a proline in a corresponding position.

As a consequence of the lateral (i.e., in the membrane plane) displacement of helices C and G, the volume of the protein transiently increases as much as 135 $Å^3$, as shown in Fig. 5B. This is twice the volume increase of the internal cavities for lumen formation described above (65 $Å^3$, Fig. 5A). Thus, the lumen does not expand only at the expense of the constriction of nearby cavities (Friedman et al, 2003), but rather is formed by a concerted "breathing" motion of the protein in which the C and G helices move semi-rigidly. The net volume change accompanying the chloride transfer ($\Delta V=V_{Product}-V_{Reactant}$) is nearly zero, consistent with what has been measured for *pharaonis* halorhodopsin by laser-induced optoacoustic spectroscopy ($\Delta V=1.73$ $Å^3$) (Losi et al, 2001) and with the dependence of the photocycle kinetics on hydrostatic pressure ($\Delta V=0$) (Váró et al, 1995a). The latter study lead to an estimation of the activation volume $\Delta V^{\ddagger}$ of ~47 $Å^3$, significantly less than the 135 $Å^3$ transient volume increase computed here for the halorhodopsin monomer. This suggests that a fraction of the lateral displacement of helices C and G is absorbed by membrane fluctuations, which is plausible since the excess volume (135-47=88 $Å^3$) is small, equivalent to the volume of about 3 water molecules.

***Role of Ser115.*** That the Ser115 hydroxyl group accompanies the chloride during the path suggests that this residue might play an essential role in the primary chloride transfer step, as already proposed (Kolbe et al., 2000). However, Fig. 4D shows that Ser115 does not contribute to lowering the energy barrier of transfer, but rather increases it by 7 kcal/mol. This finding is consistent with mutational studies of the homologous *pharaonis* halorhodopsin, in which the mutation of residue Ser130 (corresponding to Ser115) to alanine was found to not impede chloride transport (Sato et al., 2003a, Sato et al., 2003b). To clarify the role of Ser115, MEPs for the primary transfer step

were recomputed for the Ser115Ala mutant. The path with the lowest energy barrier (8.7 kcal/mol with the 'extended region' mobile) still has the chloride passing on the '115-side' of retinal. The nearly-unchanged barrier suggests that Ser115 is not important during the primary transfer step. Nevertheless, this serine is strictly conserved among halorhodopsins and therefore must play another role. Indeed, when comparing the Ser115Ala mutant to the wild-type, the reactant state is found to be destabilized by 5 kcal/mol relative to the product state. This is due mostly to loss in the reactant of the interaction between the chloride and the hydroxyl group of Ser115, which is consistent with the experimental observation that the Ser130Ala mutation lowers the chloride affinity of *pharaonis* halorhodopsin (Sato et al., 2003a, Sato et al., 2003b) and indicates that the main role of Ser115 is to increase the affinity for chloride of the binding site just below the retinal Schiff base.

***Asp238-route***. Only one MEP (path **4**) was found with chloride passing on the side of Asp238 (Fig. 3B). Its high-energy barrier of 41 kcal/mol (Table 1) means that this route is never taken. The molecular movie shows that, as the chloride moves through the three-water cluster towards Asp238, the negatively charged sidechain of the latter bends away from the approaching anion. The chloride then passes between retinal and Tyr210 (on helix F) opening a passage and thereby causing deformation of helices F and G. At the transition state the chloride is still close to Asp238, while the Schiff base twists by nearly $90^0$ so as to lower the barrier by establishing a salt-bridge with the chloride. Also, the hydroxyl group of Tyr210 makes a hydrogen bond to the chloride throughout this high-energy phase of the path. Finally, the retinal gradually untwists while the Schiff base accompanies the chloride to its product position. Energy decomposition reveals that the largest contribution to the barrier is the unfavorable electrostatic interaction between the chloride anion and the negatively-charged Asp238 (12 kcal/mol). No alternative MEP on the Asp238 side was found in which this unfavorable interaction could be avoided, so that a chloride route on that side of retinal can be excluded.

## Discussion

It has been shown here that for the primary chloride transfer step in halorhodopsin collective motion of helices C and G is necessary to allow the transient enlargement of a lumen near the Schiff base, on the Ser115 side of retinal. This involves flexible deformation of the protein up to 10 Å around the Schiff base, facilitated by a kink present in helix C. It has already been proposed that local deformation of helix C is involved in chloride translocation by halorhodopsin (Essen, 2002) and in bacteriorhodopsin proton pumping (Edman et al., 2004, Bondar et al., 2004), and that the presence of lipid molecules contribute to the elasticity of helix C (Hamilton, 2004). Indeed, in the present chloride transfer pathways palmitate is seen to accompany the flexible motion of helix C (see molecular movies). The calculated potential energy barrier of chloride passage is 9 kcal/mol, consistent with experiments indicating that the primary transfer occurs in about 1 μs (see Introduction). Other kinetic models have suggested much slower rates for the primary chloride transfer step (Dioumaev et al., 1997), but the present results show that chloride passage past retinal should be possible on the microsecond timescale. A more accurate calculation of the transfer rate will require the determination of the activation entropy and a more realistic pre-exponential rate factor than $k_BT/h$ to better account for the damped nature of the collective helix motions that are rate-limiting here. Preliminary calculations of the normal modes in the reactant and the transition state (data not shown) suggest that the vibrational entropy change contributes to somewhat accelerate the transfer rate (the formalism has been described previously by Fischer et al, 1998) in accord with the activation entropies measured for *pharaonis* halorhodopsin (Váró et al, 1995a). This reflects the increased flexibility of the protein at the transition state, probably due to a poorer packing as suggested by the transient increase in the protein volume, this effect superceding the reduced mobility of the chloride in the constricted passage during transfer.

In engineering, pump-valves often possess a spring, which keeps the valve closed and whose force must be overcome during pumping. In the case of halorhodopsin, the force required to open the lumen for chloride passage plays the role of the spring. This creates a kinetic valve that slows down chloride backflow in the resting state of the protein, while allowing chloride transfer during pumping without becoming the rate-limiting step of the photocycle. This suggests that the protein architecture is designed so as to reconcile two conflicting objectives: optimizing the productive pumping and preventing unwanted ion leakage. Protein flexibility may play a similar role in other pumps transporting sterically-demanding ions. A possible indication for this may be when the crystal structure shows no obvious passage for the ion, as is the case, for example, in the $Ca^{2+}$ ATPase (Lee, 2002, Sorensen et al., 2004). Furthermore, there might be additional valves (not necessarily kinetic ones) along the chloride pathway in halorhodopsin. One such site has been suggested for an analogous chloride pump, the Asp85Ser mutant of bacteriorhodopsin, in which Arg82 (corresponding to Arg108 in halorhodopsin) might function as a dynamical gate in chloride uptake form the extracellular side (Facciotti et al., 2003).

Path calculations performed here on the Ser115Ala mutant suggest a role for Ser115 in tuning the affinity for chloride of the binding site near retinal rather than facilitating the chloride passage itself. An analogous role is played by the corresponding residue in bacteriorhodopsin, Thr89, for which it has been shown that the photocycle of the Thr89Val mutant has wild-type levels of proton transport (Marti et al., 1991). Similarly to the present results on Ser115 in

halorhodopsin, path calculations in bacteriorhodopsin have shown that, whereas proton transfer *via* Thr89 is possible in the wild-type, the mutation to Val does not affect the energy barrier of the primary proton transfer step (Bondar et al., 2004).

## Experimental Procedures

***Protein structure.*** Protein coordinates were taken from the $HR_{578}$ ground state crystal structure (PDB entry 1E12, Kolbe et al., 2000), in which retinal is all-*trans* and residues 25-261 are solved (the solvent exposed termini are disordered). While the naturally occurring protein is probably monomeric (Steiner et al., 1983), the trimeric arrangement of the crystal was retained here since it has been observed that the protein undergoes a normal photocyle in the crystal (D.Oesterhelt, personal communication). Chloride transfer was simulated in one of the monomers. In each monomer the palmitate and 45 buried crystallographic water molecules were included, while surface water molecules were omitted. Hydrogen atoms were placed with the HBUILD facility of the program CHARMM (Brooks et al., 1983). Asp238 was considered to be deprotonated based on $pK_{1/2}$ calculations (Kolbe et al., 2000) and FTIR data showing that the protonation state of aspartic residues in halorhodopsin does not change upon chloride binding (Rotschild et al., 1998).

***Energy function***. Calculations were performed with the CHARMM force field using the all-atom parameter set 27 for the protein (MacKerell et al., 1998) and for palmitate (Feller et al., 1998). The parameters used for chloride (Roux B., 1996) and retinal (Nina et al., 1995) have been published. The bond-torsion barriers for retinal were adjusted so as to reproduce *ab initio* barriers computed for retinal analogs (Tajkhorshid et al., 2000). Non-bonded interactions were smoothly switched off between 7 and 14 Å.

Atoms within a defined region around retinal were allowed to be mobile, while the remaining atoms were kept fixed so as to avoid perturbations of the protein structure unrelated to the chloride transfer. The size of the mobile region was varied. The smallest mobile region used consisted of 46 residues around the retinal plus nearby water molecules (797 atoms) and is referred to as the 'core region'. A larger mobile region comprising the core region together with atoms situated within 6 Å around it is referred to as the 'extended region' (2178 atoms). Energy values given here were obtained with the 'extended region' unless otherwise specified.

To account for external, bulk-solvent screening effects, non-uniform charge scaling (NUCS) was applied to the system as previously described (Schwarzl et al., 2003). This method involves dividing each atomic partial charge by an individual scaling factor so as to optimally reproduce the solvated interaction energy between each group of atoms (such as a peptide group or a sidechain) and the rest of the protein as calculated by the Poisson-Boltzmann equation. For this, the halorhodopsin trimer was placed into a low-dielectric slab of 32Å thickness (centered on the N atom of the Schiff base) representing the membrane. The resulting scaling factors for the retinal and chloride are essentially equal to 1 (*i.e.*, their partial charges are unscaled).

***Pathway calculations.*** Minimum-energy paths (MEPs) were computed using the Conjugate Peak Refinement (CPR) algorithm (Fisher and Karplus, 1992) as implemented in the TREK module of CHARMM. The advantage of CPR is that it does not need the definition of an *a priori* reaction coordinate, the degrees of freedom of all mobile atoms participating in an unconstrained manner. With this method, the mechanisms of several complex reactions in proteins have been determined (Dutzler et al., 2002, Bondar et al., 2004). CPR starts from an initial guess of the path which consists of a series of structures connecting the reactant to the product. Here, many initial guesses of the path for the primary chloride transfer were made, each one built by linear interpolation from the reactant state to some putative intermediate, and from there to the product state (Fig. 3A). CPR refines the initial path by automatically adding, removing and optimizing path intermediates until all energy maxima along the connecting path segments are first-order saddle points of the surface defined by the energy function. During all path refinements the initial intermediate was removed by CPR so that it is not present in the final path (compare Figs. 3A and B). The resulting MEPs contain on average 40 conformations. Chloride transfer pathways were computed also for ground state halorhodopsin with retinal in all-*trans*. For this, the energy-minimized crystal structure was taken as the reactant state, from which the product state was built by positioning the chloride in the 'Ser115 site'.

## Acknowledgements

We are grateful to Prof. Dieter Oesterhelt for showing us the crystal structure of an $HR_{600}$ intermediate and to Dr. Walter Gmelin for helpful discussions. We thank Dr. Jerome Baudry for the retinal parameters and Mr. Nicolas Calimet for helping with the figures made with MOLSCRIPT (Kraulis P, 1991).

Received: August 4, 2004
Revised: December 23, 2004
Accepted: January 8, 2005
Published: April 11, 2005

## References

Alshuth, T., Stockburger, M., Hegemann, P.and Oesterhelt, D. (1985). Structure of retinal chromophore in halorhodopsin. A resonance Raman study. FEBS Lett. *179(1)*, 55-59.

Ames, J.B., Raap, J., Lugtenburg, J.and Mathies, R.A. (1992). Resonance Raman spectroscopy of halorhodopsin photocycle kinetics, chromophore structure, and chloride-pumping mechanism. Biochemistry *31*, 12456-12554.

Bondar, A.N., Elstner, M., Suhai, S., Smith, J.C. and Fischer, S. (2004). Mechanism of primary proton transfer in bacteriorhodopsin. Structure 12, 1281-1288.

Braiman, M.S., Walter, T.J. and Briercheck, D. M. (1994). Infrared spectroscopic detection of light-induced change in chloride-arginine interaction in halorhodopsin. Biochemistry 33, 1629-1635.

Brooks, B.R., Bruccoleri, R.E., Olafson, B.D., States, D.J., Swaminathan, S. and Karplus, M. (1983). CHARMM: a program for macromolecular energy minimization and dynamics calculations. J. Comp. Chem. 4, 187-217.

Dér, A., Fendler, K., Keszthelyi, L. and Bamberg, E. Primary charge separation in halorhodopsin. (1985). FEBS Lett. 187(2), 233-236.

Dioumaev, A. and Braiman, M.S. (1997). Nano- and microsecond time-resolved FTIR spectroscopy of the halorhodopsin photocycle. Photochem. Photobiol. 66(6), 755-763.

Dutzler, R., Schirmer, T., Karplus, M. and Fischer, S. (2002). Translocation mechanism of long sugar chains across the maltoporin membrane channel. Structure 10, 1273-1284.

Edman, K., Nollert, P., Royant, A., Belrhali, H., Pebay-Peyroula, E., Hajdu, J., Neutze, R. and Landau, E.M. (1999). High-resolution X-ray structure of an early intermediate in the bacteriorhodopsin photocycle. Nature 401, 822-826.

Edman, K., Royant, A., Larsson, G., Jacobson, F., Taylor, T., van der Spoel, D., Landau, E.M., Pebay-Peyroula, E. and Neutze

R. (2004). Deformation of helix C in the low-temperature L-intermediate of bacteriorhodopsin. J. Biol. Chem. 279(3), 2147-2158.

Essen, L.-O. (2002). Halorhodopsin: light-driven ion pumping made simple? Curr. Oppin, Struct. Biol. 12,516-522.

Facciotti, M.T., Cheung, V.S., Nguyen, D., Rouhani, S. and Glaeser, R.M. (2003). Crystal structure of the bromide-bound D85S mutant of bacteriorhodopsin: principles of ion pumping. Biophys. J. 85(1), 451-458.

Feller S.E., Yin D., Pastor R.W. and MacKerrell A.D. Jr. (1997). Molecular dynamics simulations of unsaturated lipid bilayers at low hydration: parametrization and comparison with diffraction studies. Biophys. J. 73(5), 2269-2279.

Fischer, S. and Karplus, M. (1992).Conjugate Peak Refinement: an algorithm for finding reaction paths and accurate transition states in systems with many degrees of freedom. Chem. Phys. Lett. 194(3), 252-261.

Fischer, S., Verma, C.S., Hubbard, R.E. (1998). Rotation of structural water inside a protein: calculation of the rate and vibrational entropy of activation. J. Phys.Chem.B 102,1797-1805.

Friedman, R., Nachliel, E., Gutman, M. (2003). The role of small intraprotein cavities in the catalytic cycle of bacteriorhodopsin. Biophys. J. 85(2),886-896.

Gersher, S., Mylrajan, M., Hildebrandt, P., Baron, M.-H., Müller, R. and Engelhard, M. (1997). Chromophore-anion interactions in halorhodopsin from Natronobacterium pharaonis probed by time-resolved resonance Raman spectroscopy. Biochemistry 36, 11012-11020.

Gmelin W. (2003). Strukturelle und funktionelle Untersuchungen an der lichtbetriebenen Anionenpumpe Halorhodopsin aus Halobacterium salinarum. PhD thesis.

Hamilton, J.A. (2004). Fatty acid interactions with proteins: what X-ray crystal and NMR solution structures tell us. Prog.Lipid Res. 43(3),177-199.

Ihara, K., Umemura, T., Katagiri, I., Kitajima-Ihara, T., Sugyiama Y., Kimura, Y. and Mukohata, Y. (1999). Evolution of the Archaeal rhodopsins: evolution rate changes by gene duplication and functional differentiation. J. Mol. Biol. 285, 163-174.

Kalaidzidis, I.V., Kalaidzidis, Y.L. and Kaulen, A.D. (1998). Flash-induced voltage changes in halorhodopsin from Natronobacterium pharaonis. FEBS Lett. 427, 59-63.

Kolbe, M., Besir, H., Eseen, L.-O. and Oesterhelt, D. (2000). Structure of the light-driven chloride pump at 1.8 Å resolution. Science 288, 1390-1396.

Kraulis, P. (1991). MOLSCRIPT: a program to produce both detailed and schematic plots of protein structures. J. Appl. Cryst. 124, 946-950.

Lanyi, J.K. (1984). Light-dependent trans to cis isomerization of the retinal in halorhodopsin. FEBS Lett. 175(2), 337-342.

Lanyi, J.K. (1990). Halorhodopsin, a light-driven electrogenic chloride-transport system. Physiol. Rev. 70(2), 319-330.

Lee, A.G. (2002). A calcium pump made visible. Curr. Opin. Struct. Biol. 12(4),547-554.

Losi, A., Wegener, A.A., Engelhard, E. and Braslavsky, S.E. (2001). Thermodynamics of the early steps in the photocycle of Natronobacterium pharaonis halorhodopsin. Influence of the medium and of anion substitution. Photochem. Photobiol. 74(3), 495-503.

Ludmann, K., Ibron, G., Lanyi, J.K. and Váró, G. (2000). Charge motions during the photocycle of pharonis halorhodopsin. Biophys. J. 78, 959-966.

MacKerell, A.D. Jr., Bashford, D., Bellot, M et al. (1998). All-atom empirical potential for molecular modeling and dynamics studies of proteins. J. Phys. Chem. 102, 3586-3616.

Marti, T., Otto, H., Mogi, T., Rösselet, S.J., Heyn, M.P. and Khorana, H.G. (1991). Bacteriorhodopsin mutants containing single substitution of serine or threonine residues are all active in proton translocation. J. Biol. Chem. 266(1), 6919-6927.

Mukohata, Y., Ihara K., Tamura, T. and Sugyiama Y. (1999). Halobacterial Rhodopsins. J. Biochem. 125(4), 649-657.

Nina, M., Roux, B. and Smith, J.C. (1995). Functional interactions in bacteriorhodopsin: a theoretical analysis of retinal hydrogen bonding with water. Biophys. J. 68, 25-39.

Oesterhelt, D., Hegemann, P. and Tittor, J. (1985). The photocycle of the chloride pump halorhodopsin. II: Quantum yield and a kinetic model. EMBO J. 4(9), 2351-2356.

Oesterhelt, D. Structure and function of halorhodopsin. (1995). Isr. J. Chem. 35, 475-494.

Rotschild, K.J., Bousche, O., Braiman, M.S., Hasselbacher, C.A. and Spudich, J.L. (1998). Fourier transform infrared study of the halorhodopsin chloride pump. Biochemistry 27, 2420-2424.

Roux B. (1996). Valence selectivity of the gramicidin channel: a molecular dynamics free energy perturbation study. Biophys J. 71, 3177-3185.

Rüdiger, M. and Oesterhelt, D. (1997). Specific arginine and threonine residues control anion binding and transport in the light-driven chloride pump halorhodopsin. EMBO J. 16(13), 3813-3821.

Sato, M., Kikukawa, T., Araiso, T., Okita, H., Shimono, K., Kamo, N., Demura, M. and Nitta, K. (2003a). Ser-130 of Natronobacterium pharaonis halorhodopsin is important for the chloride binding. Biophys. Chem. 104, 209-216.

Sato, M., Kikukawa, T., Araiso, T., Okita, H., Shimono, K., Kamo, N., Demura, M. and Nitta, K. (2003b). Roles of Ser130 and Thr126 in chloride binding and photocycle of pharaonis halorhodopsin. J. Biochem. 134, 151-158.

Schobert, B. and Lanyi, J.K. (1982). Halorhodopsin is a light-driven chloride pump. J. Biol. Chem. 257(17), 10306-10313.

Schobert, B., Lanyi, J.K. and Oesterhelt, D. (1984). Effects of anion binding on the deprotonation reactions of halorhodopsin. J. Biol. Chem. 262(2), 2690-2696.

Schwarzl S., Huang D., Smith J.C. and Fischer S. (2003). How well does charge reparametrisation account for solvent screening in molecular mechanics calculations? The example of myosin. In Silico Biology 3, 187-196.

Sorensen, T.L., Moller, J.V. and Nissen, P. (2004). Phosphoryl transfer and calcium ion occlusion in the calcium pump. Science 304(5677), 1672-1675.

Steiner, M. and Oesterhelt, D. (1983). Isolation and properties of the native chromoprotein halorhodopsin. EMBO J. 2(8), 1379-1385.

Tajkhorshid, E., Baudry, E., Schulten, K. and Suhai, S. (2000). Molecular dynamics study of the nature and origin of retinal's twisted structure in bacteriorhodopsin. Biophys. J. 78, 683-693.

Váró, G., Needleman, R. and Lanyi, J.K. (1995a). Light-driven chloride ion transport by halorhodopsin from Natronobacterium pharaonis. 2. Chloride release and uptake, protein conformation change and thermodynamics. Biochemistry 34, 14500-14507.

Váró, G., Zimanyi, L., Fan, X., Sun, L., Needleman,R. and Lanyi, J.K. (1995b). Photocycle of halorhodopsin from Halobacterium salinarium. Biophys. J. 68, 2062-2072.

Walter, T. and Braiman, M.S. (1994). Anion-protein interactions during halorhodopsin pumping: halide binding at the protonated Schiff base. Biochemistry 33, 1724-1733.

Warshel, A. (1978). Charge stabilization mechanism in the visual and purple membrane pigments. Proc. Natl. Acad. Sci. USA 75(6),2558-2562.